An Automated Ladar Polarimetric System for Remote Characterization of Space Materials

*George C. Giakos,***Richard. H. Picard, **** Willa Inbody, ****Phan D. Dao, ****Peter N. Crabtree, ****Patrick J. McNicholl, *Jeff Petermann, *Suman Shrestha, *Chaya Narayan, and **Stefanie Marotta
*Dept. of Electrical and Computer Engineering,
**Dept. of Biomedical Engineering
The University of Akron, Akron, OH 44325-3904, USA
***ARCON Corporation, Waltham, MA 02451
****Air Force Research Laboratory, Space Vehicles Directorate
Kirtland AFB, NM 87111, USA

Abstract— **The calibration, testing, and operational principles of an efficient multifunctional monostatic polarimetric ladar are introduced and related to the system performance metrics. The depolarization, diattenuation, and retardance of the materials were estimated using Mueller matrix (MM) decomposition for different aspect angles. The outcome of this study indicates that polarimetric principles may enhance the capabilities of the ladar to provide adequate characterization and discrimination of unresolved space objects.**

Keywords- Calibration Techniques, Mueller Matrix Decomposition, Space Materials, Discriminant Signatures

I. INTRODUCTION

Accurate sensing of small and distant satellites as well as the discrimination of these satellites from natural near-earth objects and man-made debris is still a challenging and important space remote-sensing task, along with the prediction of interactions between and threats to these space objects. Polarimetric sensing and imaging offer unique advantages for a wide range of detection and classification problems due to the intrinsic potential for high contrast in different polarization components of the backscattered light.[1]-[2], [7]-[12], [15]-[16], [18]-[21].

This study presents the calibration, testing, and operational principles of an efficient laboratory testbed multifunctional monostatic ladar polarimetric system aimed at enhancing the detection, identification, characterization, and discrimination of unresolved space objects at different aspect angles. The performance of the ladar system has been tested against known space materials, namely, amorphous silicon (AS), and polysilicon (PS). The system exhibited excellent accuracy. The uniqueness of this study consists in applying polar decomposition of space materials at varying aspect angles, under diffuse reflectance geometry.

Originally, space borne remote sensing applications have traditionally involved radars utilizing advanced synthetic aperture radars [1]. Within this content, RF polarimetry has proven effective for characterizing Earth features such as geological processes, meteorological forecasting, agricultural activities planning, and climate model validation [2]. Several studies investigated the use of polarimetry in X-ray band [3]. On the other hand, the progress of the lightwave technology, the introduction of solid state lasers, the availability of new wavelengths between 1100-1550 nm, and the development of the photonics industry, contributed to the development of ladar remote sensing applications and optical communication systems. Interestingly enough, the polarimetric formalisms of both RF and optical polarimetry have been studied extensively in [15]-[16], and [17]-[18], respectively. Advances of optical polarimetry for remote sensing applications have been achieved in the area of image enhancement. Hooper et al [4] studied an airborne imaging system consisting of multiple cameras that could take images remotely in several spectral bands along with three separate polarizations. Although their method did not utilize full polarimetric measurements, however degrees of Linear Polarization (DOLP) images were shown to highlight marine features of interest with greater specificity. Similarly, Wang et al [5] utilized polarimetric properties to estimate refractive indices of materials. As a further enhancement, algorithms were explored to evaluate the angle of incidence within the framework of the pBRDF, or polarization bi-directional reflectance distribution function, commonly used in many geophysics studies. Hyde et al [6] provides greater details of the pBRDF used in that study. In another study, Giakos demonstrated that enhanced images can be obtained, by fusing multispectral and polarimetric principles. The same study suggested the possibility of increased and reconfigurable depth resolution for biomedical applications [7].

Several studies have contributed great theoretical significance to this study. Liu et al [8] developed a system that utilized

liquid crystal devices, LabVIEW, PC Control, and CCD Images. Giakos et al [9] introduced polarimetric wavelet detection principles aiming at enhanced detection and discrimination of remote objects. Additional LC systems were discussed by Bueno [11] and Chipman [12], with main emphasis on system calibration and accuracy. Both studies conducted calibration tests on known samples such as air, reflectors, and linear polarizers. The results of [10]-[11] were helpful in establishing benchmarks for calibration used in this study.

A powerful technique used in this study is the Lu-Chipman algorithm [12]-[13] which decomposes MM data into constituent matrices representing specific properties. The isotropic and anisotropic depolarization of materials using polar decomposition was studied by Le Roy-Brehonnet et al [14]. Specifically, the net depolarization, also referred to in literature as the depolarization index, was applied as a signature to discriminate among a group of materials consisting of dielectrics, granite, polished steel, and nylon.

II. THEORETICAL FORMALISM

The polarimetric measurements were obtained under diffuse reflectance geometry. The optical system consists of two arms, namely the generator and the analyzer. The generator comprises all the optical polarimetric components, including the source prior to interaction with the object, while the analyzer refers to all polarimetric components after the object including the detector.

Efficient calculations of the Mueller matrix (MM) of the objects have been performed using data reduction technique [12]. In order to determine the 16 elements of a Mueller matrix of an object, 16 linearly dependent equations must be estimated; therefore, a minimum of 16 measurements must be made; this has been achieved by generating at least 16 polarimetric states, at selected generator-analyzer configurations, so that 16 measurements were obtained, one per each polarimetric state; As a result, a system of equations was generated which allowed the MM of the object to be determined, in terms of 16 MM elements; each of the 16 MM elements is expressed uniquely in terms of the 16 polarimetric states.

MM decomposition, expressed as sequence of three matrix factors, namely, the depolarization, retardance, and diattenuation, was originally proposed by Shih-Yau Lu and Russell Chipman.[12]-[13]. This concept can be expanded for Bidirectional Reflectance Distribution Function (BRDF) applications by expressing them in terms of the aspect angle of an object, θ, so that

$$M(\theta) = M_{depol}(\theta) M_{ret}(\theta) M_{diat}(\theta) \quad (1)$$

$M_{depol}(\theta)$ accounts for the depolarizing effects of the medium, $M_{ret}(\theta)$ accounts for the retardance effects of linear birefringence and optical activity, and $M_{diat}(\theta)$ describes the effects of linear and circular dichroism. From these matrices the diattenuation, retardance, and depolarization characteristics of the medium are readily determined.

The depolarization is quantified in terms of the depolarization index, P_D, according to

$$P_D(\theta) = Dep\left(M(\theta)\right) = 1 - \frac{\sqrt{\left(\sum_{i,j} m_{i,j}^2(\theta)\right) - m_{11}^2(\theta)}}{\sqrt{3} m_{11}(\theta)} \quad (2)$$

where $m_{ij}(\theta)$ are the MM elements as a function of the aspect angle. From the decomposed retardance matrix, $M_{ret}(\theta)$, the total retardance, R, which includes the effects of both linear and circular birefringence, can be expressed as

$$R(\theta) = \cos^{-1}\left(\frac{tr\left(M_{ret}(\theta)\right)}{2} - 1\right) \quad (3)$$

where $tr\left(M_{ret}(\theta)\right)$ is the trace of the retardance matrix. The diattenuation, d, is dependent on the first row vector of the MM. This vector describes differential attenuation for both linear and circular polarization states and the diattenuation can be expressed in terms of it as

$$d(\theta) = \frac{1}{m_{11}(\theta)} \times \sqrt{m_{12}^2(\theta) + m_{13}^2(\theta) + m_{14}^2(\theta)} \quad (4)$$

III. EXPERIMENTAL DESIGN

The LC polarimeter consists of the following components:

1. **Generator arm:** The incident laser light is initially linearly polarized by **a fixed polarizer** at +45°.
2. The light then passes through a **compensated variable retarder** (polarization **rotator**) that is capable of producing all linear polarization states, including but not limited to horizontal, vertical, and ±45°.
3. The light then passes through a **variable retarder**, which is capable of producing right and left circularly polarized light.

4. The light then impinges on the target, and the diffusely reflected light is collected by the analyzer arm.
5. **Analyzer arm:** The analyzer arm consists of the same components as the input arm except in reverse order and with the fixed polarizer set at -45°.

Before the system could be used for experimental purposes, the retarder and the rotator must be calibrated four different states, namely: horizontal polarization, vertical polarization, $+45^0$ polarization and Right Circular polarization states; these states are used on the generator and the analyzer arm to generate 16 different states for the computation of 16 different intensities required for the Mueller matrix calculation. Hence, the required voltage for the retarder and the rotator must be estimated and applied so that these liquid crystal components work in the desired polarization state. As the voltage is applied across the liquid layer, the molecules rotate towards the direction of the applied electric field, which introduces retardance such that different polarization states are achieved. A LabVIEW subroutine is developed to control the retarder and the rotator in the desired state required for the experiment.

The calibration technique consists of a two-step procedure. The first step requires the voltage calculation of the retarders and rotators. The second step involves the accuracy test of the calibrated voltages by using it to determine the Mueller matrix of elements which have known Mueller matrices.

1) System Calibration:

Accurate alignment is critical to the polarimetric system accuracy. The system components are aligned collinearly in a line-of-sight transmission geometry as shown in Fig 1. As each component is added, the appropriate voltages are applied until rotation or retardation is achieved. Once the generator states are obtained, the analyzer components are added and the process is repeated to determine their operational voltages. To verify the state of polarization at the detector, the polarizer at the analyzer arm is always included in the arrangement [17].

Calibration is obtained by using a method called *Null-Intensity Method* where the polarizer at the analyzer arm is always kept under cross-polarized geometry to the polarizer in the generator arm and the voltage is applied to each of the liquid crystal devices such that the null intensity is obtained [10], [17]. Because of the presence of limited system noise in the experiment, the accurate location of the true null is difficult to observe. Thus, a different method is used, namely, the "*Method of Swings*" [17]. In this new method, the polarizer at the analyzer arm is rotated by small angle $\Delta\theta$ to measure the intensities at $90+\Delta\theta$ and $90-\Delta\theta$. When these two measurements are equal, the null exactly in between these angles is the calibration voltage.

2) System Testing:

After the liquid crystal devices (retarders and rotators) are calibrated, these calibration voltages are first tested using some objects of known Mueller matrices.

The experimental setup used for the system qualification (accuracy test) is as shown in Fig 2.

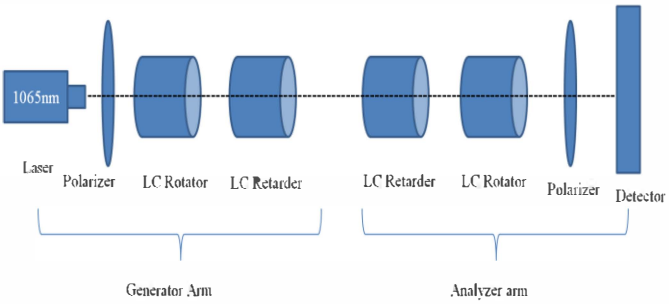

Figure 1. System calibration arrangement

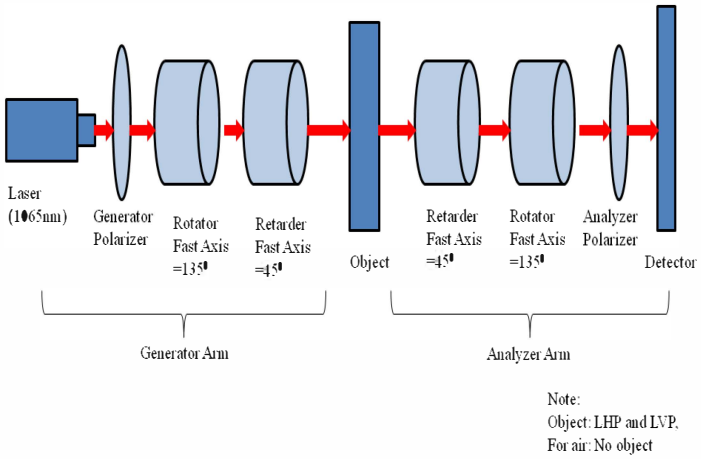

Figure 2. System testing arrangement with emitter and receiver settings, polarizer, rotator (fast axis = 135^0), retarder (fast axis = 45^0) in the generator arm, and the same in reverse order in the analyzer arm with object to be tested between the generator and analyzer arms.

These test experiments are done in transmission mode, i.e., placing the generator and the analyzer arm in the line-of-sight. Between the generator and the analyzer arm, the object to be tested is placed. The polarizer (linear horizontal and linear vertical) used for the experiment is specified for the wavelength range between 700nm-1100nm which is within the range of the laser that is being used.

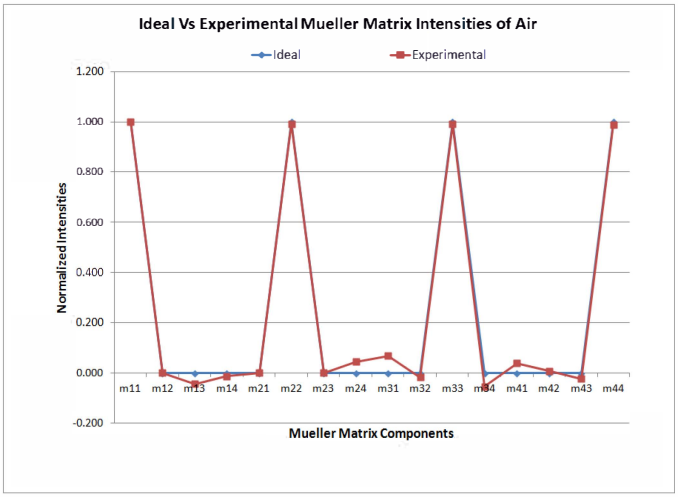

(a)

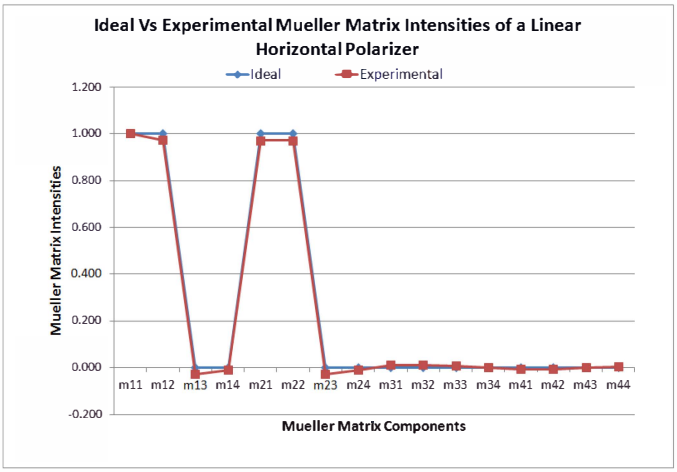

(b)

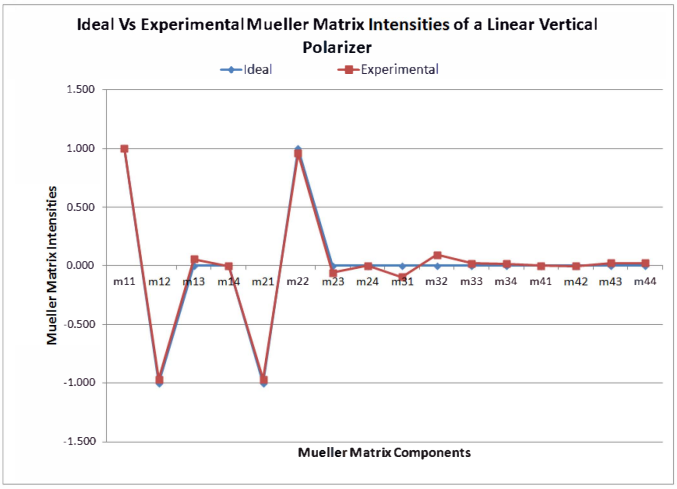

(C)

Figure 3. Comparison of ideal and experimental MM intensities of a) air, b) a linear horizontal polarizer, and c) a linear vertical polarizer

The MM is then calculated using the system setup for three objects—air, a linear horizontal polarizer, and a linear vertical polarizer--and their calculated values are compared with the ideal values. The plots of the ideal and the experimental values of the MM for the three objects used for the system qualification are shown in Fig. 3.

3) Experimental Arrangement

The experimental arrangement is shown in Fig 4. Here, the generator and analyzer arms are not collinear and samples are measured in a reflective mode. Optical measurements are obtained at sixteen different polarization states as mentioned earlier, with a combination of four polarization states in the generator and the analyzer arm. The acquired waveforms with their respective histograms are then recorded using a 7000 Series LeCroy Wave Analyzer, and then processed using Excel and MATLAB subroutines for analysis.

The MM of the materials is derived for many known angles (aspect angles or tilt angles) spanning a range of +/- θ about the on-axis location. The generator and the analyzer arms are kept very close together. Additionally, a large enough distance to the object is used so that specular reflection angle approaches 0^0. A very slight tilt is introduced to the analyzer to further approach 0^0.

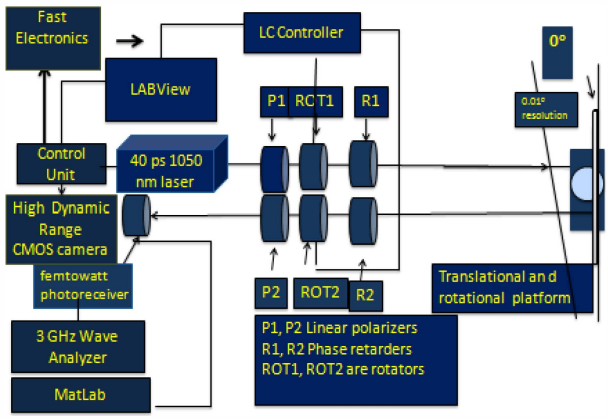

Figure 4. The U.S. Air Force Research Laboratory (AFRL) multifunctional imaging platform

This approximates the conditions in which the device would need to operate in an actual scenario. The experiment is performed at different aspect angles. For this, the object is rotated from its normal incidence angle in the positive and negative direction. Rotation is achieved with the help of a stepper motor with 0.01^0 resolutions. In this study, the angle of maximum intensity for a co-polarized intensity is considered to be the on-axis condition or 0^0.

IV. Results And Discussions

Using the experimental arrangement of Fig 4, backscattered light intensities from the samples are obtained. A comparison of MM of the object at normal incidence is shown below where the abbreviations, AS and PS, represent the amorphous silicon and polysilicon, respectively. It is interesting to note that significant difference between the two different forms of silicon is observed along the diagonal of the matrix, which represents isotropic absorption.

$$M_{AS} = \begin{bmatrix} 1 & .00 & .04 & -.01 \\ .00 & .99 & .08 & -.10 \\ -.03 & .10 & -.98 & .37 \\ -.02 & -.01 & -.21 & -.91 \end{bmatrix} \quad M_{PS} = \begin{bmatrix} 1 & .01 & .03 & .05 \\ .01 & .93 & .08 & -.18 \\ -.05 & .19 & -.91 & .15 \\ .05 & -.07 & -.12 & -1 \end{bmatrix}$$

Next, Mueller matrices are compared at various angles of rotation. The MM element intensities at selected angles are shown in Figures 5 and 6. The bars in the graph are ordered from negative to positive angles of peak magnitude 11° through zero degrees. Each MM element shows a relatively high degree of symmetry regardless of the direction of rotation.

Next, decomposition parameters obtained by the Lu-Chipman Algorithm [12]-[13] are grouped by material and analyzed as a function of object rotation angle in Figs 7-8. The maximum measured intensity for a co-polarized generator-

analyzer combination is plotted as a reference since this is a good indicator of maximum reflection. This condition for all materials is obtained with a generator-analyzer combination of HH or VV (i.e. both the generator and analyzer arm kept at horizontal polarization or vertical polarization state), although HH is chosen as the reference for plotting.

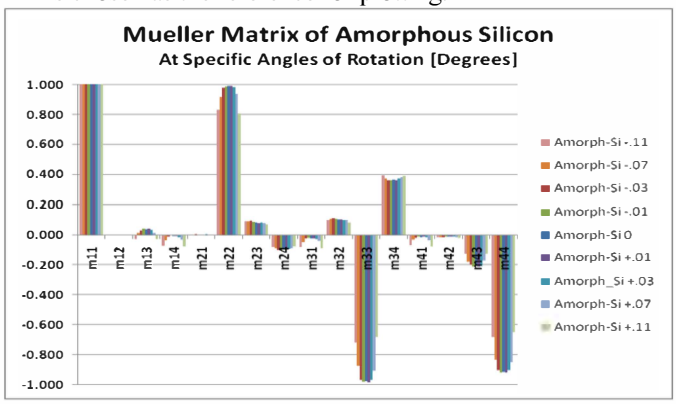

Figure 5. MM of amorphous silicon at selected angles.

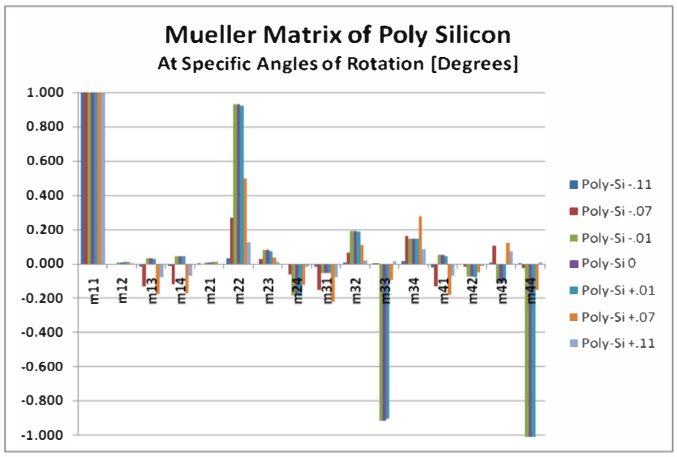

Figure 6. MM of polysilicon at selected angles

For comparison purposes, the diattenuation magnitude, retardance in radians, and the net depolarization are plotted in Figs, 7-8. Under normal circumstances, diattenuation would not be defined at non-normal angles. In this study however, the goal is to find useful discriminators for characterization of the material and its orientation. In this scenario, numerical values of diattenuation may not be critical so examination of its general behavior is justifiable. The results for amorphous silicon and polysilicon are shown in Figs. 7-8, respectively. Since a large amount of data is plotted simultaneously, it is to be noted the color coding of the scales for easier comparisons. The vertical axis on the left side serves as a scale for three parameters with the same color as is used in the legend. The vertical axis on the right only refers to retardance (purple). Some observations can be made, namely:

i) Minimum depolarization correlates well to the angle of normal incidence (pronounced specular reflection).

ii) The depolarization increases for both the materials with increasing the aspect angle proportionally (increased diffuse reflectance).

iii) The order of materials from least depolarizing to most depolarizing is: amorphous silicon and poly-silicon. In fact, It has been shown earlier that enhanced specular characteristics is associated with amorphous silicon while polysilicon, exhibits pronounced diffuse scattering [9].

iv) The retardance stayed very much constant in general for both the materials.

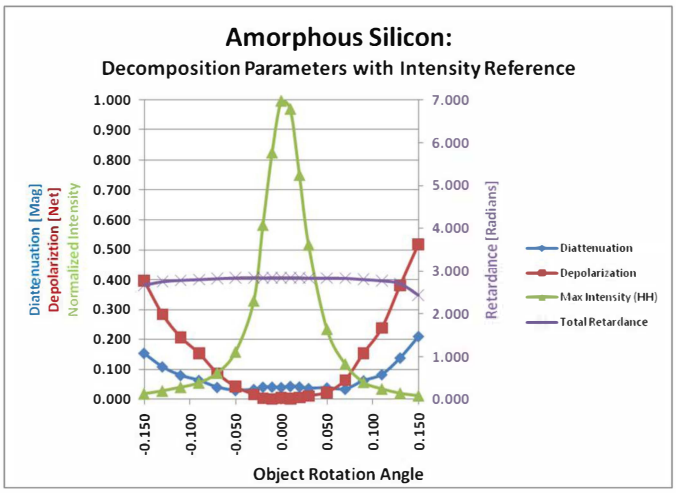

Figure 7. Decomposition parameters vs object rotation angle for amorphous silicon

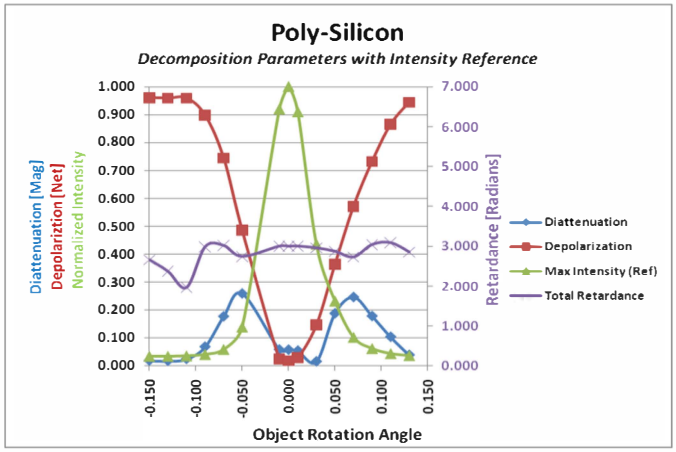

Figure 8. Decomposition parameters vs object rotation angle for polysilicon

For further analysis, the decomposition coefficients are compared by their optical property. Specifically, both materials are plotted on the same graph for each individual coefficient. Note that the scale used for some of the following plots is decreased to exaggerate the behavior of the property. The diattenuation (magnitude), net depolarization and total retardance are shown in Figures 9, 10, and 11 respectively.

V. CONCLUSION

A new and efficient polarimetric detection technique for the characterization of space materials has been presented. The outcome of this study indicates that the material's optical characteristics, namely, diffuse scattering, diattenuation magnitude, net depolarization and retardance have been used

as potential discriminants among different objects. Indeed, the system, under which the experiment was performed, exhibited excellent accuracy.

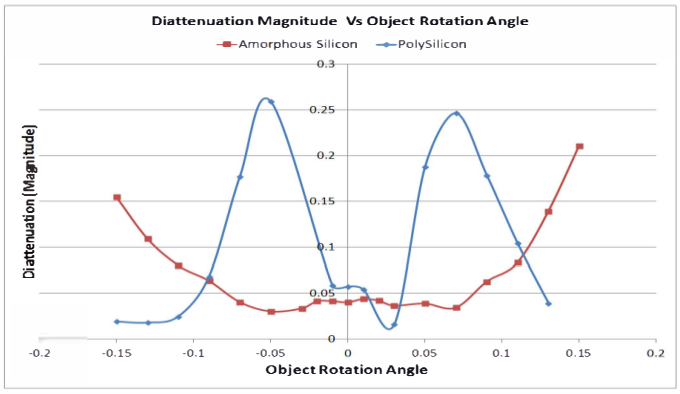

Figure 9. Diattenuation magnitude vs object rotation angle for both materials.

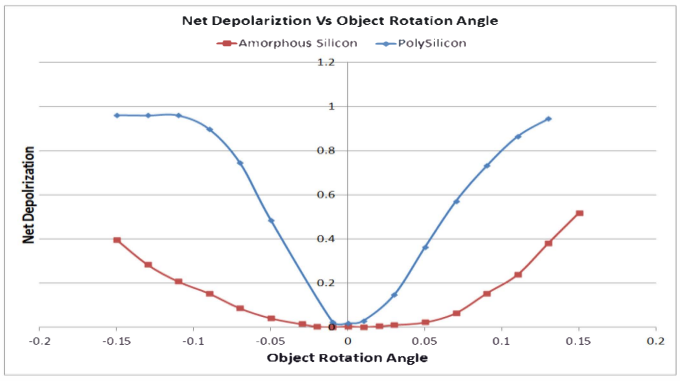

Figure 10. Net depolarization vs object rotation angle for both materials

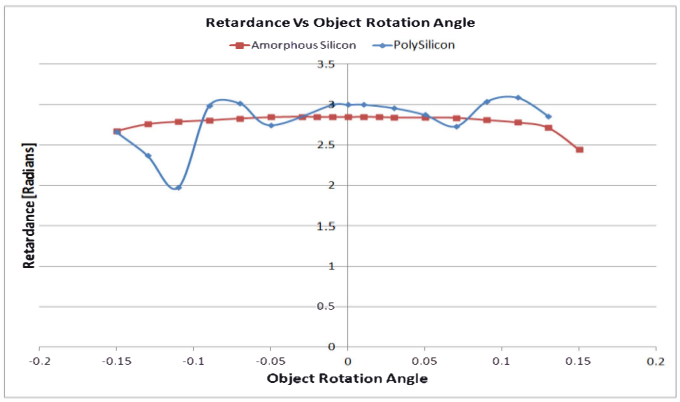

Figure 11. Total retardance vs object rotation angle for both materials

ACKNOWLEDGEMENT

G. C. Giakos and R. H. Picard gratefully acknowledge that this study was performed under contract with the U.S. Air Force Research Laboratory (AFRL).

REFERENCES

[1] "Space-borne imaging," Aerospace and Electronic Systems Magazine, IEEE , vol.15, no.10, pp.118-124, Oct 2000.

[2] A. Breuer, I. Hajnsek, "Analytical Solution for Polarimetric Surface Scattering Model," Proc. of POLinSAR Workshop 2003.

[3] R.. M. Curado da Silva, N. Auricchio, E. Caroli, A. Donati, M. Hage-Ali, F. Schiavone, P. Siffert, J. B. Stephen, G. Vcntura, "Hard-X and soft gamma ray polarimetry with CdTe array prototypes," Nuclear Science Symposium Conference Record, 2003 IEEE , vol.5, no., pp. 3606- 3611 Vol.5, 19-25 Oct. 2003.

[4] B. A. Hooper, B. Baxter, C. Piotrowski, J. Z. Williams, J. Dugan,, "An Airborne imaging Multispectral Polarimeter (AROSS-MSP)" OCEANS 2009, MTS/IEEE Biloxi - Marine Technology for Our Future: Global and Local Challenges , vol., no., pp.1-10, 26-29 Oct. 2009.

[5] Qingsong Wang, C. D. Creusere, V. Thilak, D. G. Voelz, "Active Polarimetric Imaging for Estimation of Scene Geometry," Digital Signal Processing Workshop and 5th IEEE Signal Processing Education Workshop, 2009. DSP/SPE 2009. IEEE 13th , vol., no., pp.659-663, 4-7 Jan. 2009.

[6] M. Hyde, J. Schmidt, and M. Havrilla, "A geometrical optics polarimetric bidirectional reflectance distribution function for dielectric and metallic surfaces," Opt. Express 17, 22138-22153 (2009).

[7] G. C. Giakos, "Multifusion Multispectral Lightwave Polarimetric Detection Principles and Systems," Instrumentation and Measurement, IEEE Transactions on , vol.55, no.6, pp.1904-1912, Dec. 2006

[8] G. L. Liu, Y. Li, and B. D. Cameron, "Polarization-based optical imaging and processing techniques with application to cancer diagnostics", Proceedings of SPIE, Vol.4617, pp.208-220, 2002.

[9] .G. C. Giakos, R. H. Picard, P. D. Dao, P. N. Crabtree, P. J. McNicholl, "Polarimetric Wavelet Phenomenology of Space Materials", IEEE International Conference on Imaging Systems and Techniques, Batu Ferringhi, Malaysia, IEEEXplore, pp.1-6, 17-18 May 2011.

[10] J. S. Baba, J. Chung, A. H. Delaughter, B. D. Cameron, G. L. Cote, "Development and calibration of an automated Mueller Matrix Polarization Imaging System, Journal of Biomedical Optics 7(3), 341-349, July 2002.

[11] J. M. Bueno, "Polarimetry Using Liquid Crystal Variable Retarders: Theory and Calibration", J. Opt. A: Pure Appl. Opt. 2, 2000.

[12] R. A. Chipman, " Polarimetry Handbook of Optics", Journal of Biomedical Optics, 2nd edition (New York: McGraw-Hill), vol. 2, chapter 22, February 2010

[13] Shih-Yau Lu and Russell A. Chipman, "Interpretation of Mueller matrices based on polar decomposition," J. Opt. Soc. Am. A **13**, 1106-1113, 1996.

[14] F. Le Roy-Brehonnet, B. Le Jeune, P. Y. Gerligand, J. Cariou and J. Lotrian, "Analysis of depolarizing optical targets by Mueller matrix", Formalism, *Pure Appl. Opt.* 6 385, 1997.

[15] W. M. Boerner, H. Mott, E. Luneburg,, "Polarimetry in remote sensing: basic and applied concepts," Geoscience and Remote Sensing, 1997. IGARSS '97. Remote Sensing - A Scientific Vision for Sustainable Development., 1997 IEEE International , vol.3, no., pp.1401-1403 vol.3, 3-8 Aug 1997.

[16] E. K. Colin, "Polarimetric optical tools and decompositions applied to SAR images," Geoscience and Remote Sensing Symposium, 2007. IGARSS 2007. IEEE International , vol., no., pp.4191-4194, 23-28 July 2007

[17] D. Goldstein, "Polarized Light" 2nd Ed., Marcel Dekker Inc, New York, 2003.

[18] J.R. Shell II, S.D. Brown, M.G. Gartley, and J.R. Schott, Fundamentals of Polarimetric Remote Sensing, SPIE Press, 30 March 2009.

[19] D. Goldstein, National Technical Information Services, Department of Defense, Air Force Research Laboratory, Munitions Directorate, (2003, Februatry), Polarization Signature Research, Eglin AFB FL.

[20] G. Giakos, R. Picard, and P. Dao, "Superresolution multispectral imaging polarimetric space surveillance LADAR sensor design architectures", SPIE vol. 207, pp. 71070B-71070B-12, 2008.

[21] G. C. Giakos, "Advanced Detection, Surveillance, and Reconnaissance Principles", Proc. IEEE International Workshop on Measurement Systems for Homeland Security, pp. 6 – 10, Orlando, FL, 2005.